Article

Anthropogenic Influence on the Antarctic Mesospheric Cooling Observed during the Southern Hemisphere Minor Sudden Stratospheric Warming

Sunkara Eswaraiah [1,2,*], Kyong-Hwan Seo [1,3,*], Kondapalli Niranjan Kumar [4], Madineni Venkat Ratnam [5], Andrey V. Koval [6], Jin-Yun Jeong [2], Chalachew Kindie Mengist [1], Young-Sook Lee [7], Katelynn Greer [8], Jun-Young Hwang [7], Wonseok Lee [9], Maniyattu Pramitha [10], Gasthi Venkata Chalapathi [11], Mannem Venkatarami Reddy [3] and Yong Ha Kim [6]

1   Research Center for Climate Sciences, Pusan National University, Busan 46241, Korea
2   Satellite Research Centre, Madanapalle Institute of Technology and Science, Madanapalle 517325, India
3   Department of Atmospheric Sciences, Pusan National University, Busan 46241, Korea
4   National Centre for Medium Range Weather Forecasting, Noida 201301, India
5   National Atmospheric Research Laboratory, Department of Space, Gadanki 517112, India
6   Atmospheric Physics Department, Saint Petersburg State University, 198504 Saint Petersburg, Russia
7   Department of Astronomy and Space Science, Chungnam National University, Daejeon 34134, Korea
8   Laboratory for Atmospheric and Space Physics, University of Colorado, Boulder, CO 80303, USA
9   Department of Atmospheric Sciences, Yonsei University, Seoul 03722, Korea
10 Indian Institute of Science Education and Research, Trivandrum 695551, India
11 Department of Physics, Government Degree College, Ananthapuramu 515001, India
*   Correspondence: eswar.mst@gmail.com (S.E.); khseo@pusan.ac.kr (K.-H.S.)

Abstract: Processes behind Sudden Stratospheric Warming (SSW), which occurs more frequently in the northern hemispheric polar latitudes and its influence from the stratosphere to the upper atmosphere are well documented. However, physical processes associated with SSW, although it ensues rarely in the southern hemisphere (SH), have a strong influence on the background atmosphere from the stratosphere to the mesosphere and are poorly understood. Using a ground-based meteor radar, satellite-borne Microwave-Limb sounder, and Modern-Era Retrospective Analysis for Research and Applications observations, we identified cooling of Antarctic mesopause by 26 K in response to a 66 K warming in the polar stratosphere during the 2019 minor SSW in the SH. The observed cooling is attributed to the interplay between planetary waves, CO_2 infrared cooling, and O_3 depletion, rather than adiabatic cooling due to gravity waves alone during SSW. It is proposed that anthropogenic and other sources generating chemical tracers in the lower atmosphere have caused mesospheric cooling and could be transported from the lower atmosphere both vertically and meridionally through residual mean meridional circulation from the tropics. Therefore, our study for the first time demonstrates the effect of lower atmosphere chemistry on the polar mesosphere thermal structure during the 2019 SSW.

Keywords: sudden stratospheric warming; mesospheric cooling; meteor radar; planetary waves; chemical species transport; residual mean meridional circulation

1. Introduction

The recent National Aeronautics and Space Administration (NASA) study observed that the rising human-made greenhouse gas emissions and the growing climate change menace have caused shrinking of the upper atmosphere, especially the mesosphere region (50–100 km) due to its cooling [1]. A 1–2 K cooling in the mesosphere per decade (~100–200 m shrinking of the mesosphere) in response to an increase in greenhouse gas (carbon dioxide (CO_2), and ozone (O_3)) emissions has been noted. They also reported that the sudden stratospheric warming (SSW) is too a cause of the mesosphere cooling and shrinking of

the upper atmosphere. Hence, the present study aimed and is designed to understand the physical mechanisms liable for the enhancement of the anthropogenic gases that are responsible for mesospheric cooling during a southern hemisphere (SH) SSW event.

The sudden stratospheric warming (SSW) phenomenon [2] has invited a significant amount of consideration in recent years owing to its role in changing the Earth's middle and upper atmospheric structure and dynamics on a large scale in both hemispheres [3]. SSWs occur six times per decade in the Northern Hemisphere (NH) [4], whereas in the SH, they seldom occur because of less topographic forcing and smaller planetary wave (PW) amplitudes [5]. After the 2002 major SSW [6,7], two minor SSW events in 2010 [8] and 2019 [9–11] were recorded in the SH.

The 2019 SSW in the SH demonstrated prominent effects on Antarctic mesospheric dynamics, through winds, waves, and tides [9,11]; however, the polar mesospheric temperature response has not yet been examined. Eswaraiah et al. [12] observed that polar mesospheric cooling (PMC) tele-connects to other regions of the globe through mean circulation during SSWs. Therefore, the evaluation of PMC during SSWs is of significant importance for understanding global atmospheric circulation. However, the meticulous mechanism of PMC is not yet fully understood. It is believed that the gravity wave (GW) force affects the general circulation in the mesosphere and leads to PMC during SSW, and this mechanism was used in [13,14]. In contrast, mesospheric cooling was also observed in the absence of GWs [15], which could be due to locally generated tropospheric PWs and their upward propagation, and their influence on mean circulation changes in the mesosphere. However, in 2019 SSW, a weak/suppressed GW force was observed [16] due to the wind-filtering effect in the stratosphere [10]; consequently, mesospheric cooling may not be due to GWs. Hence, the present study attempted to find the other possible reasons for PMC apart from GW force-induced dynamical cooling.

Earlier studies [17–19] suggested that mesospheric cooling can also be instigated by the natural minor chemical constituents present in the mesosphere itself or transported from the remote atmospheric regions through wave modulations, and PW-induced meridional circulation during the SSW. In recent years, the importance of residual mean meridional circulation (RMC) in transporting greenhouse gas species from the lower atmosphere to other regions of the atmosphere has been well-recognized by considering the wave impacts on chemical species' transport [20,21]. Among all the greenhouse gases, CO_2 disrupts the mesospheric thermal structure at a larger scale [1]; hence, the thermal (dynamical) and chemical connection between the Earth's surface-atmosphere and mesosphere strengthened in recent years due to global warming. Therefore, the present study aims to unravel the principal mechanism of Antarctic mesospheric cooling during the 2019 SSW. In doing this, we revealed the role of anthropogenically emitted greenhouse gases (chemical species) in mesospheric cooling and their vertical and meridional transport in association with the upward-propagated PWs and RMC.

Further, continuous ground-based observations of mesospheric temperature studies during the SH SSWs are scarce [22,23]. In the present study, for the first time, we report the Antarctic mesospheric temperature during the 2019 minor SH SSW, using simultaneous observations from ground-based meteor radar (MR) at the KSS station (62.22° S, 58.78° W) (KSSMR) along with the Microwave Limb Sounder (MLS) and Modern-Era Retrospective Analysis for Research and Applications (MERRA).

2. Data and Methods

2.1. Data

The present study makes use of temperature, and zonal and meridional winds in the stratosphere and mesosphere with three different datasets covering ground-based, satellite, and reanalysis. The ground-based King Sejong Station (62.22° S, 58.78° W) Meteor Radar (KSSMR) was used to measure the mesospheric temperature and winds. The KSSMR provides winds from 70–100 km with a 1 h and 2 km height resolution, and temperature estimates are available at 90 km [8,24]. The mesospheric temperature profiles over

Antarctica and the variability of chemical species (CO, O_3) in the middle atmosphere were obtained from observations of the Earth Observing System (EOS) MLS onboard the Aura satellite version 4.2 Level 2 data [25]. In addition to the KSSMR and MLS, we also used the Modern-Era Retrospective Reanalysis for Research and Applications-2 (MERRA-2) [26] for temperature, winds, CO evaluation and circulation analysis. MERRA-2 (referred to as MERRA in the text) is the latest version of the modern satellite package produced by the NASA Global Modeling and Assimilation Office (Greenbelt, USA). MERRA data are available over $0.625° \times 0.5°$ longitude–latitude grids at pressure levels ranging from 500 hPa to 0.01 hPa.

2.2. Methods

2.2.1. KSSMR Temperature

Usually, meteor radar temperatures are estimated using the conventional temperature gradient method or pressure assumptions method at a peak meteor detection height; however, the difficulty involved in these techniques is that the methods always depend on other models. The unique method used in the study utilizes the linear relationship between the full width at half maximum (FWHM) of the meteor height distribution at two different heights where the peak meteor rate exists and the temperature at the meteor peak height. This method provides the continuous mesopause temperature with better precision rendering to the measurements of the FWHM alone without any additional information [24].

The FWHM of two different heights, Z1 and Z2, is directly proportional to the temperature within these height layers, and can be written as follows:

$$\text{FWHM} = \frac{R}{g} \ln\left(\frac{\rho_1}{\rho_2}\right) \langle T \rangle$$

where FWHM = Z2 − Z1, and R and g are the gas constant and gravitational acceleration, respectively. The constants ρ_1, and ρ_2 are the densities of the atmosphere at Z1 and Z2.

The height layer mean temperature $\langle T \rangle$ between the two constant pressure levels $\rho_1(Z_1)$ and $\rho_2(Z_2)$ is defined as follows:

$$\langle T \rangle = \int_{\rho_1}^{\rho_2} T d \ln\rho \Big/ \int_{\rho_1}^{\rho_2} d \ln \rho$$

2.2.2. Residual Mean Meridional Circulation

In the present study, we used the transformed Eulerian mean (TEM) circulation method [20] in order to overcome the limitations [21] that existed in the earlier mean Eulerian meridional circulation approach. The present method (TEM) effectively affords diagnostics of wave impacts on the mean flow and is useful to estimate the meridional transport of mass and tracers in the atmosphere.

The residual mean meridional circulation (RMC) used in the study is a superposition of eddy-induced and advective zonal-mean flows. The meridional and vertical components of the RMC were estimated using the TEM approach [20]. However, the original TEM method equations were slightly modified to obtain a more convenient form.

$$\overline{v}^* = \overline{v} - \frac{1}{\partial\overline{\theta}/\partial z}\left(-\frac{\overline{v'\theta'}}{H} + \frac{\partial\overline{v'\theta'}}{\partial z} - \frac{\overline{v'\theta'}}{\partial\overline{\theta}/\partial z}\frac{\partial^2\overline{\theta}}{\partial z^2}\right),$$

$$\overline{w}^* = \overline{w} + \frac{1}{a\cos\varphi}\frac{1}{\partial\overline{\theta}/\partial z}\left(-\sin\varphi\,\overline{v'\theta'} + \cos\varphi\left(\frac{\partial\overline{v'\theta'}}{\partial\varphi} - \frac{\overline{v'\theta'}}{\partial\overline{\theta}/\partial z}\frac{\partial^2\overline{\theta}}{\partial z\partial\varphi}\right)\right).$$

where $\overline{v}^*$, $\overline{w}^*$ are residual meridional and vertical velocity components. The overbars denote the zonal-mean values, the dashes mark the deviations of hydrodynamic quantities from their zonal-mean values $v' = v - \overline{v}$; $\theta' = \theta - \overline{\theta}$; v and w are the meridional and vertical components of wind; ρ is the background atmospheric density; z is the vertical log-isobaric

coordinate; θ is potential temperature; φ is latitude; a is the Earth's radius; and H is the pressure scale height.

2.2.3. Wavelet Spectral Analysis

To see the vertical extent of planetary waves in the temperature and their presence in the mesospheric meridional winds, the daily mean temperatures from the stratosphere to the mesosphere obtained from MERRA, and mesospheric meridional winds measured by KSSMR from 1 July to 15 October 2019, were subjected to "Morlet" wavelet analysis.

3. Results and Discussions

3.1. Antarctic Mesosphere Response to the 2019 SSW

The 2019 minor SSW in the SH was registered on August 30 and reached its peak on 17 September 2019, during which the SH polar stratosphere experienced a drastic warming phase (~66 K), with a significant change in the zonal mean zonal winds (~72 m/s) at 10 hPa and 62.5° S (Figure S1a,b), greater than that of the 2002 major SSW [9]. The PWs of zonal wavenumber1 (PW1) were abnormally amplified in the stratosphere at 62.5° S, achieving a record maximum amplitude (highest amplitude in the last 40 years) during the 2019 SH winter [9] (Figure S1c,d). Lim et al. [10] proposed that these (PW1) waves are the main drivers of the weakening of the polar vortex and the formation of the 2019 SSW.

The Antarctic mesospheric temperature variation in response to the drastic increase in stratospheric (~32 km) temperature during the 2019 SSW is displayed in Figure 1. The KSS meteor radar-measured mesospheric temperature at 90 km is shown in Figure 1a, and the middle mesospheric temperatures (75 km) measured using MLS and MERRA are displayed in Figure 1b. The variability of polar stratospheric temperature at 32 km is shown in Figure 1c. The climatological mean and standard deviation are also shown in each panel. The mesospheric temperature measured by the meteor radar showed a maximum cooling of ~26 K at ~90 km (Figure 1a), while the middle mesosphere (~75 km) cooled by up to ~24 K (Figure 1b) in response to a significant increase in the polar stratospheric (~32 km) temperature (~66 K) during the peak SSW (Figure 1c). The radical surge in the stratospheric temperature (~66 K) observed in the 2019 SH SSW relative to the 40-year normal (Figure 1c) was ~16 K greater than the 2002 SH major SSW that persisted for a week [9]. It is intriguing to note that the magnitude of the mesospheric cooling observed during the 2019 minor SSW was higher than that observed in the 2002 major SSW [23] and the 2010 minor SSW in the SH [8]. Another implication of the 2019 SSW is the vertical extent of mesospheric cooling. The KSS meteor radar temperature measurements during the 2019 SSW showed that the vertical extent of mesospheric cooling was noted until ~90 km (Figure 1a), while in the 2002 major SSW it was observed for up to ~80 km [27]. This is quite interesting since the 2002 SSW was a major event while that of 2019 was a minor warming event.

3.2. Plausible Physical Mechanisms Responsible for Mesospheric Cooling

The increasing trend of the anthropogenic emission of greenhouse gases, such as carbon dioxide (CO_2), carbon monoxide (CO), and ozone (O_3), plays a crucial role in the thermal energy budget of the atmosphere [28] due to their long chemical lifetime. Earlier studies [29] suggest that due to the large mixing ratio of chemical tracers that exist in the atmosphere, the dynamical forcing of atmospheric waves could affect the transport of heat and chemical species to the middle and upper atmosphere from below. Further, the dissipation of waves at different altitudes of the atmosphere generates diffusive mixing coefficients both in the meridional and vertical dimensions and modulates the transport of heat and chemical species [29]. So, to ascertain the possible reasons for the mesospheric cooling during the 2019 minor SSW, we evaluated the chemical species (CO and O_3) and their possible infrared cooling of the mesosphere, and the role of PWs in causing PMC through the change in circulation.
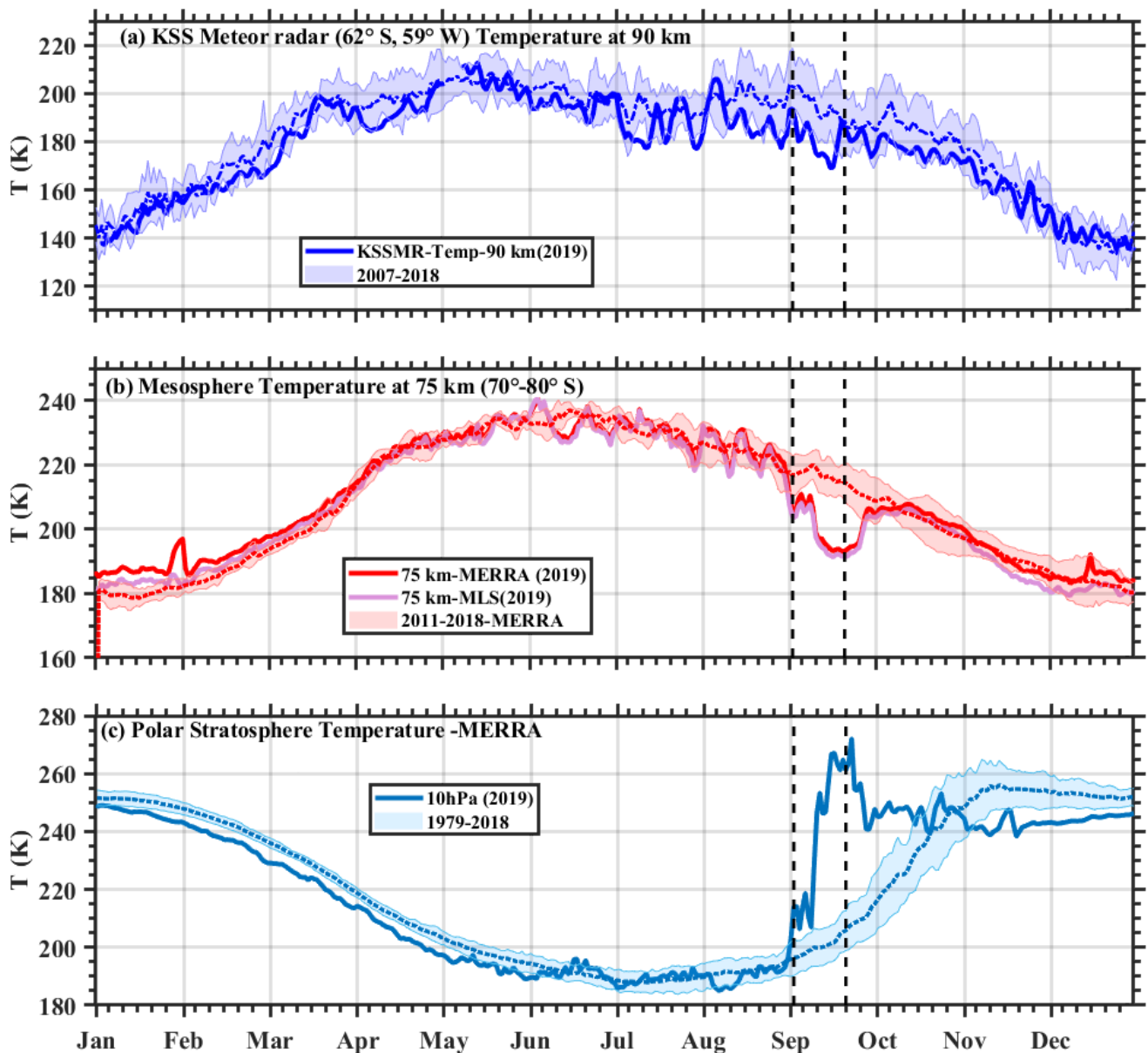
Figure 1. Daily mean variability of the (**a**) mesospheric temperatures at ~90 km obtained using KSS meteor radar (62° S, 59° W), and (**b**) at ~75 km using MLS and MERRA over 70°–80° S. (**c**) Polar stratospheric temperature at 10 hPa (~32 km) in the SH obtained from MERRA. In each panel, the temperature during 2019 is shown along with the climatological mean (dashed lines) and standard deviation (shaded areas). The vertical dashed lines indicate the onset and peak SSW days.

3.2.1. Chemical Species-Induced Mesospheric Cooling

To illustrate the chemical species distribution and its connection to temperature variability both in the stratosphere and mesosphere, polar stereographic polar projection maps using the MLS satellite observations are shown in Figure 2. The maps are shown at different isentropic surfaces (potential temperatures) and their equivalent altitude level is also shown in the figure. Greater warming in the polar stratosphere at ~32 km (10 hPa) (Figure 2a) and cooling at ~50 km and in the mesosphere at ~75 km are noted. The cooling is significant at mesospheric altitudes at all longitudes in the SH polar region (Figure 2c). The O_3 concentration is moderately high at ~50 km (Figure 2e) as a natural phenomenon with an abrupt fall in the mesosphere (Figure 2f). A spike in the CO mixing ratio was noted at 32 km (Figure 2g) over the western side of the Antarctic and the tip of South America, and the resultant variations in T and O_3 can be seen at 32 km (Figure 2a,d). However, CO

was less pronounced in the upper stratosphere (Figure 2h) and significantly enhanced in the mesosphere (Figure 2i). The changes in T, O_3 and CO are indicated by the arrows. The decline in O_3 and the enhancement in CO concentration over the polar region are indicative of mesospheric cooling (Qian et al., 2013). However, Garcia et al. [30] reported that CO_2 and CO, and to some extent O_3, are responsible for the high levels of radiative cooling of the mesosphere and lower thermosphere (MLT) [31].
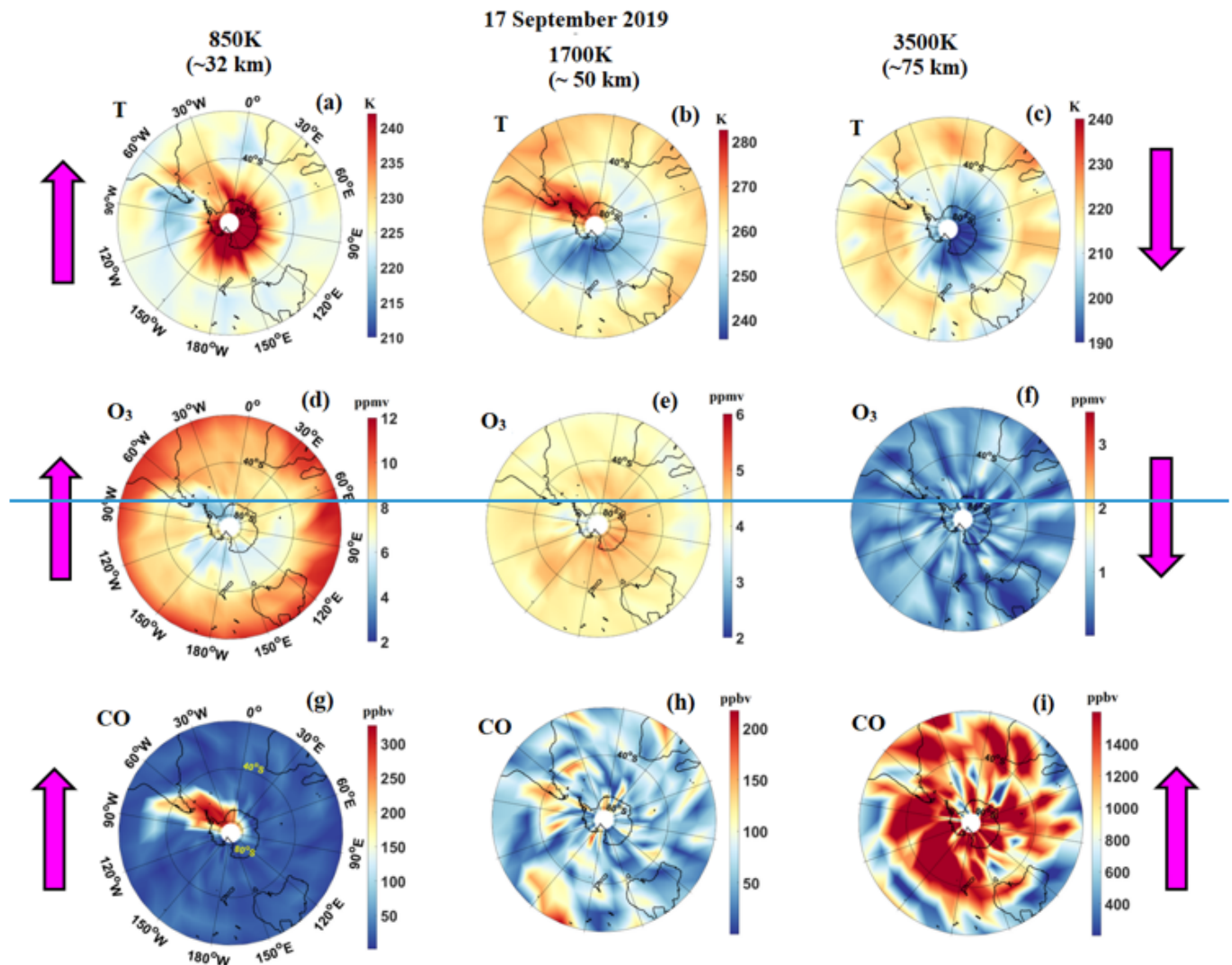
Figure 2. The polar projection of the stratospheric (~32, and 50 km) and mesospheric (~75 km) temperature (**a–c**), ozone (O_3) (**d–f**), and carbon monoxide (CO) (**g–i**) during the peak warming day using MLS observations. The maps are shown at different isentropic surfaces (potential temperatures). The upward magenta color arrows show the increasing value, and the downward arrow is indicative of decreasing.

To quantify the mesospheric cooling due to CO, the daily variability of CO from MERRA and mesospheric temperatures using MERRA, and MLS over the SH polar region (70°–80° S) is depicted in Figure 3. Figure 3a shows the daily variability of CO at 75 km along with the climatological mean and standard deviation, and the variability of the polar mesospheric temperature in response to changes in CO during the SSW period is displayed in Figure 3b. From the figure, it is apparent that there was a strong anti-correlation between the mesospheric temperature and CO concentration during the SSW period. CO increased from 25 August and was at its highest level between the onset (30 August) and peak (17 September) SSW, and largely departed from its climatological

mean. Additionally, CO is a byproduct of CO_2, produced from the photolysis of CO_2 at wavelengths <121 nm. Thus, a high CO mixing ratio implies the existence of abundant CO_2 in the mesosphere. Nevertheless, photolysis causes a very minor decrease in the budget of CO_2 in the mesosphere [30]. Therefore, the higher incidence of mesospheric cooling is due to increased CO_2 and its infrared emission, as well as partly due to O_3 depletion.
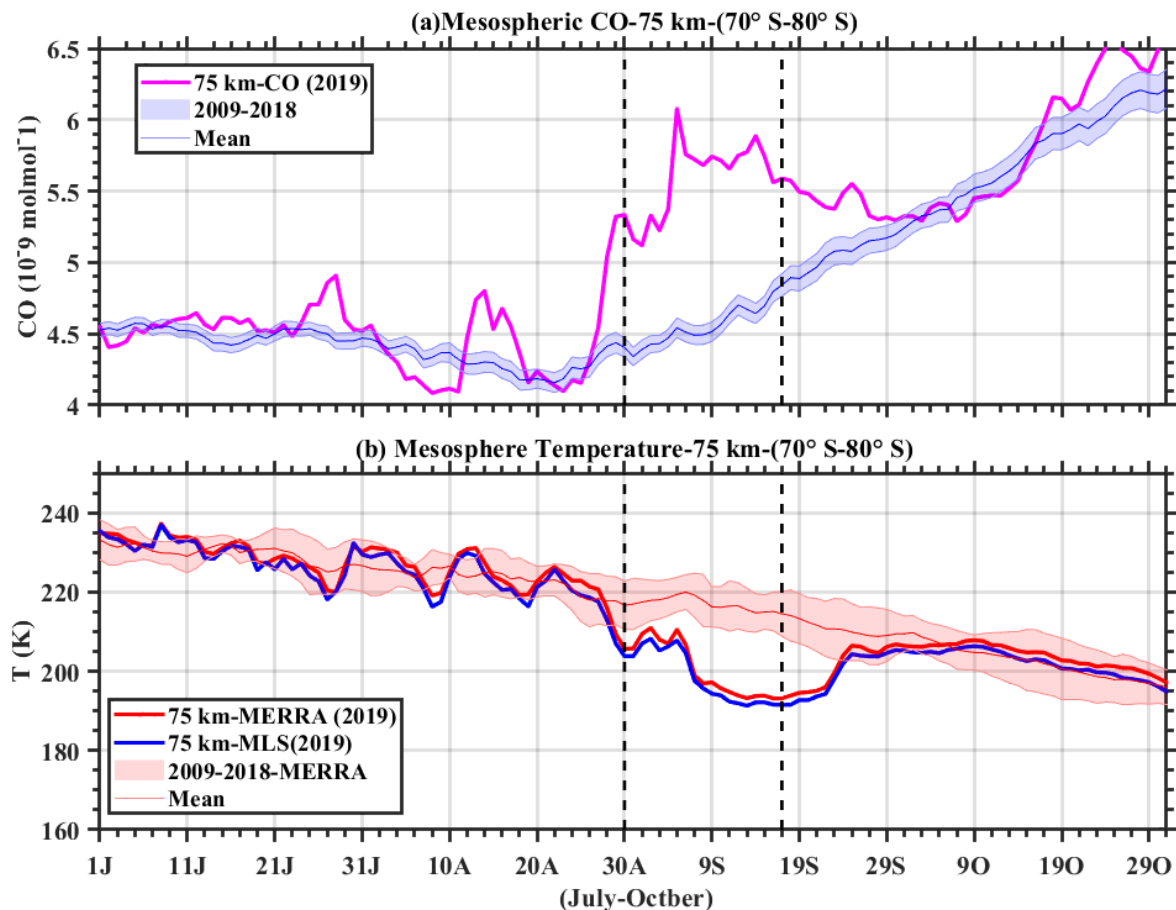

Figure 3. (**a**) Daily mean variability of the carbon monoxide (CO) at ~75 km using MERRA. (**b**) Same as (**a**) but for temperature variability obtained using both MERRA and MLS over 70°–80° S. The vertical dashed lines indicate the onset and peak SSW days.

3.2.2. Planetary Wave Propagation: Mesospheric Cooling

It has been proposed that the existence of PWs in the mesosphere will change the meridional circulation, thereby inducing mesospheric cooling [15,32]. To see the manifestation of PWs in the mesosphere and their connection to the temperature variations, the radar measured meridional winds in the mesosphere and MERRA temperatures in the stratosphere and mesosphere were subjected to wavelet spectral analysis [33] for the SSW period (1 July to 30 September 2019) and the resultant spectra are shown in Figure 4. The observed PWs in the radar winds at 80 km are shown in Figure 4a; furthermore, the PW signatures in MERRA temperatures in the mesosphere (80 km, 75 km) and the stratosphere (32 km) are shown in Figure 4b–d, respectively. It is evidenced from the figure that PWs with a period of 10 days (8–12-day peak at 10 days) are significantly presented in radar-measured mesospheric meridional winds (Figure 4a) and the stratospheric (Figure 4d) and mesospheric temperatures (Figure 4b,c) during SSW. In addition to 10-day PWs, we also observed shorter (<5 days) PWs in the temperature during the SSW from 32 km to 80 km. It is worth noting that PWs with a 10-day period were significant and strong at 32 km in the stratospheric temperature during the onset of the SSW event (Figure 4d) and their amplitude decreased with height (Figure 4b,c). This, in turn, suggests that 10-day PWs

propagate from below into the mesosphere; therefore, they might alter the mesospheric temperature and wind structure [15,32]. The source of the PWs could be located in the mid-latitude troposphere due to surface heat flux driven by the mid-latitude Rossby wave train [34,35]. Hence, there is a possible connection between mesospheric cooling and PW propagation during SSW.
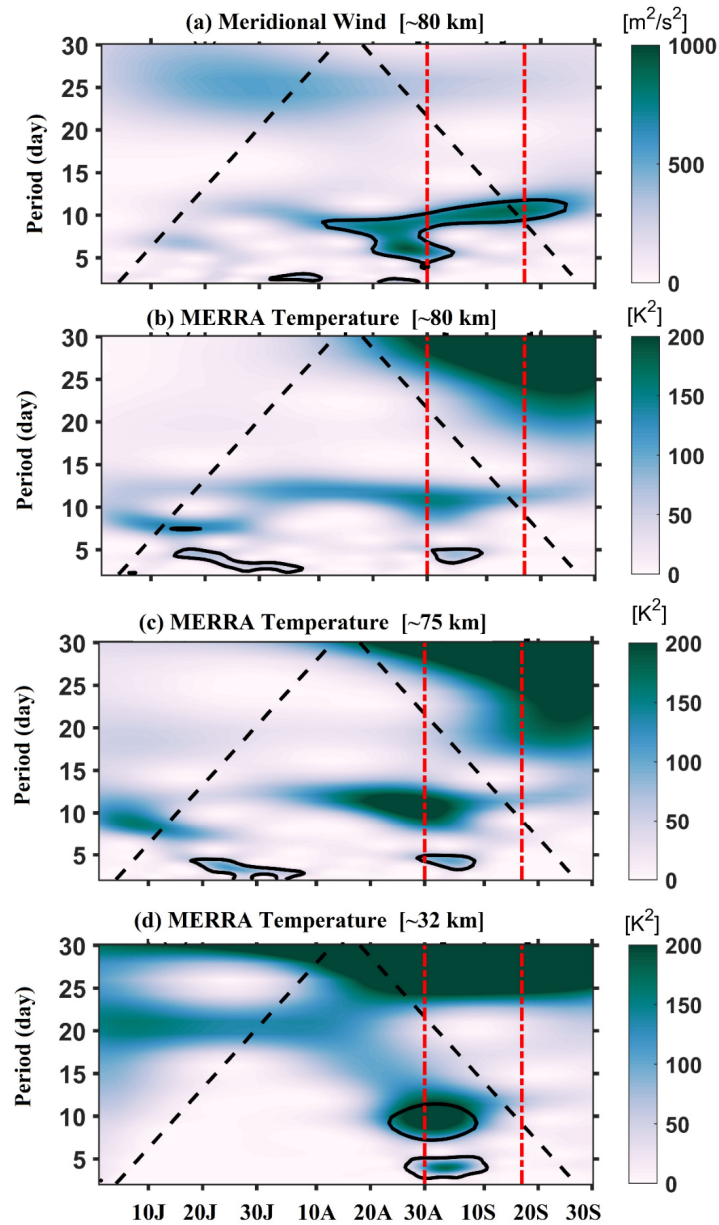

Figure 4. (**a**) Continuous wavelet spectrum of the KSS MR measured meridional winds at 80 km between 1 July and 30 September 2019, (**b**–**d**) same as (**a**), but for the temperature using MERRA data over KSSMR (62.22° S, 58.78° W), at 80 km, 75 km, and 32 km, respectively. The dashed black line in the wavelet spectrum shows the cone of influence. The vertical dashed lines indicate the onset and peak SSW days. The thick black contours indicate the significant periods of the planetary waves.

3.2.3. Residual Mean and Wave-Induced Eddy Meridional Circulation: Mesospheric Cooling

It has been reported that the greenhouse gases, especially CO_2, emitted by anthropogenic or natural sources in the tropical lower atmosphere [36] are transported upward and poleward by PWs-induced residual mean meridional circulation (RMC) and act as one of the major drivers of polar mesospheric temperature variability [18,21]. The RMC during the 2019 SH winter was estimated with the method described in Koval et al. [21] using

MERRA data. The RMC is a superposition of the mean Eulerian and wave-induced eddy components [20,21]. The meridional and vertical components of the RMC were estimated according to the Transformed Eulerian Mean (TEM) approach [21,37]. In addition to RMC, we also estimated eddy fluxes and wave-induced eddy meridional circulation during the same interval of RMC as depicted in Figure 5.
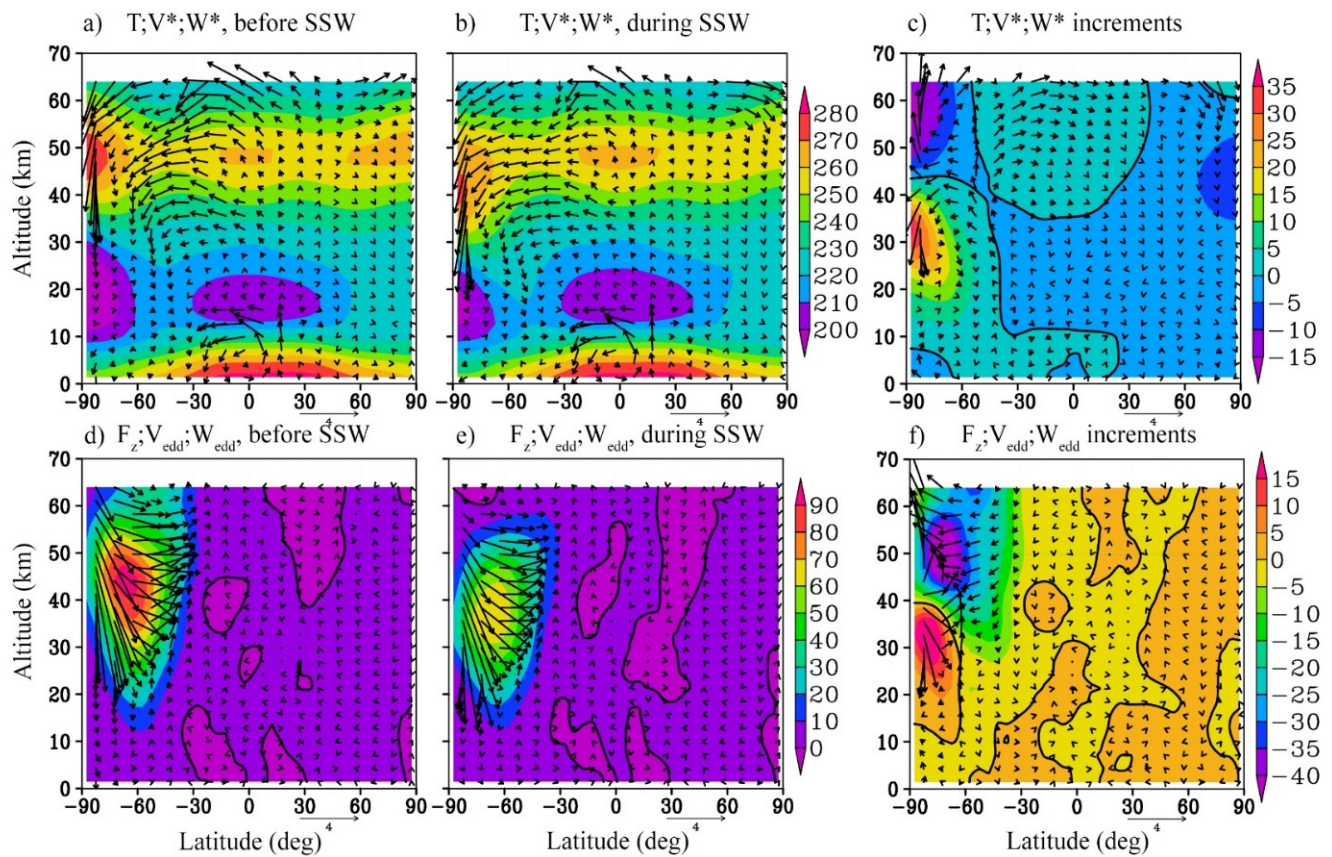
Figure 5. (**a**) Latitude-height distributions of temperature (shaded) and the residual mean circulation (RMC) components (m/s, arrows) before the peak SSW (**a**): ten-day average from 26 August–5 September 2019). (**b**) Same as (**a**) but during the SSW peak (6–19 September 2019). (**c**) changes between the specified parameters (**a,b**). (**d,e**) show Fz (10^4 m^3/s^2, shaded) and wave-induced eddy meridional circulation (m/s, arrows) during the same time intervals as (**a,b**). (**f**) changes between the specified parameters (**d,e**). Where V*, W* are residual meridional and vertical velocity components. The vertical component of the circulation is multiplied by 200.

The top panels of Figure 5 show the residual circulation and temperature before the peak SSW (26 August–5 September) (Figure 5a) and during the peak SSW (6–19 September) (Figure 5b) and their difference (Figure 5c). Before and during the SSW, the planetary wave-induced RMC cells were upward and poleward in the SH upper stratosphere and downward in the polar region (Figure 5a,b). Due to MERRA data limitations, we are unable to show the RMC above 70 km; however, the vectors show a tendency towards the winter pole (SH) (Figure 5a,b). Usually, above 70 km in the mesosphere, single cell circulation is detected [20]. The difference in RMC (Figure 5c) shows the downward vertical velocity components in the lower stratosphere resulting in adiabatic heating around 10 hPa (32 km), and upward velocity in the upper stratosphere and lower mesosphere causing cooling. The downward velocity components of RMC in the subpolar upper stratosphere are much stronger in Figure 5a; hence, the difference has more of an upward flux (Figure 5c) and results in cooling in this region (above 50 km). In addition, in the tropical troposphere, the dominant upward and poleward cell structure was noted before and after the SSW, showing the tropical Hadley cells controlled by diabatic heating [38]. Additionally, the

upward-propagating PWs modulate the air motion through eddy diffusion or dissipation and could support the transport of chemical species (CO_2, O_3, and other trace gases) to the polar region [39]. Hence, we also estimated the PW-induced eddy circulation.

The bottom panels of Figure 5 show the PW-induced eddy circulation, calculated using formulas from Koval et al. [21] (arrows) and the vertical component of the Eliasson–Palm flux (E-P flux) for the same time intervals. Figure 5d shows PWs-induced eddy-circulation before the SSW, Figure 5e represents this during the SSW and Figure 5f represents their difference. The EP flux describes the propagation direction of the wave, and the divergence of EP flux is more suitable for estimating the effect of the wave on the background. Moreover, according to the formula for the E-P flux [37], the upward E-P flux corresponds to the poleward wave heat flux. Accordingly, its weakening also weakens the heating of the polar region in the mesosphere. Figure 5f shows the respective increments. It can be seen that above 40 km the E-P vertical flux weakens during the SSW peak. The downward eddy flow also weakens (upward directed arrows). At the same time, in the circumpolar region between 15 and 40 km, reverse effects are observed—an increase in the ascending E-P flux, which enhances heat transfer to the polar stratosphere, and an acceleration of the descending eddy circulation, which contributes to additional adiabatic heating of this region. All these processes are interpreted as the impact of PW on the mean flow.
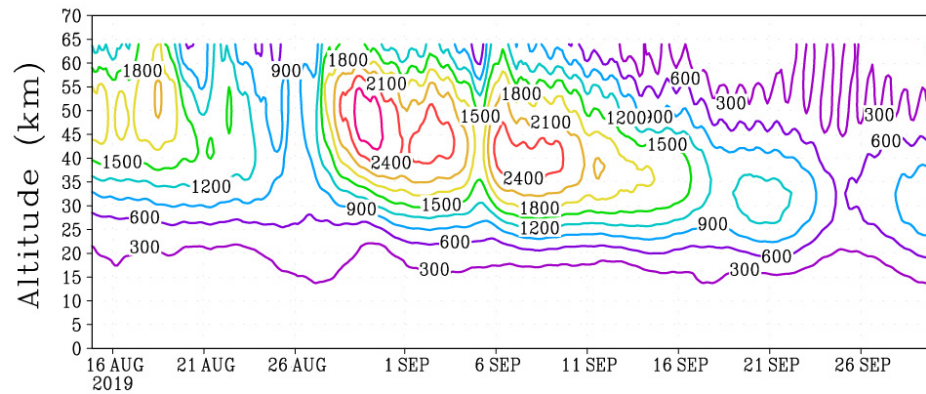
It is further suggested that [18] PWs with zonal wavenumbers 1–3, can propagate vertically and meridionally and play a dominant role in the transport of chemical species via the modulation of upward airflow and meridional circulation. However, in the present SSW, PWs with zonal wave numbers 1 and 2 (PW1 and PW2) are the strongest waves [9,10]. So, to ascertain the PW features from the surface to mesosphere in the SH polar region, the time series of the amplitudes of PW1 and PW2 averaged over latitudes of 60°–80 °S using MERRA are shown in Figure 6a,b, respectively. The time-altitude profiles of the deviation of the mean temperature at 82°–87° S are depicted in Figure 6c. It can be seen that during the entire SSW (26 August–19 September) there is an increase in the amplitudes of these waves, and during the peak of the SSW (6–19 September) the wave maximum descends, which is accompanied by a weakening of the E-P flux in the mesosphere and the cooling of this region (Figure 6c). This is a purely dynamic effect that causes changes in the temperature of the subpolar region during the SSW.

Though there is less land surface area over the SH, CO_2 emissions originating primarily from Australian wildfires [40] and Southern Ocean outgassing [41] are transported to the polar region. Thus, our investigations suggest that the mesospheric cooling that occurred during the 2019 SH SSW could be the consequence of upward propagated PWs and radiative cooling induced by chemical species.
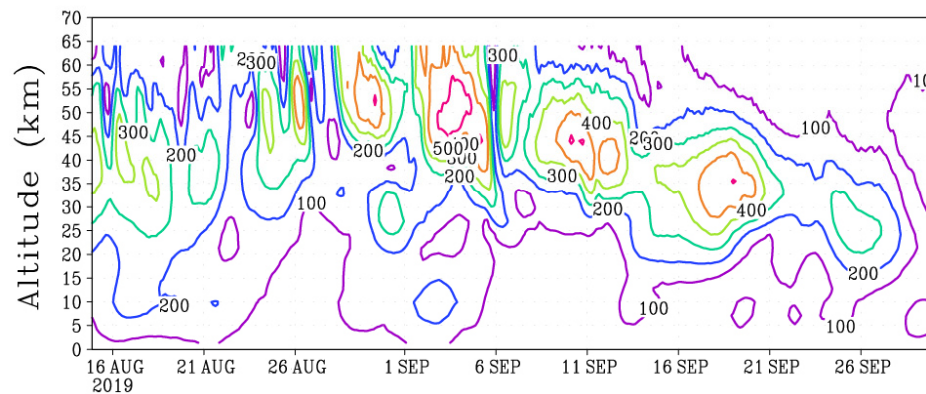
The overall mechanism of mesospheric cooling during the 2019 SH SSW is presented in a simple schematic sketch in Figure 7. The anomalous amplification of PW1 in the SH polar region led to the establishment of a minor SSW and strong warming in the stratosphere. As discussed above, the 10-day PWs generated in the lower atmosphere during the SSW and that propagate upward to the mesosphere could induce a change in the meridional circulation which in turn changes the mesosphere temperature. The chemical tracers generated in the tropical region are transported to the polar stratosphere and mesosphere through the residual mean meridional circulation. Below 70 km, the residual circulation is upward over the tropical region and downward over the winter polar (SH) region (Figure 5a,b); and above 70 km in the mesosphere, summer to winter residual circulation occurs during the SH winter [18,21,42]. The downward residual circulation in the stratosphere (mesosphere) induces warming (cooling) [18,20]. The upward-propagating PWs over the polar region could also transport the chemical species from the lower atmosphere [39]. Thus, an abundant amount of CO_2 accumulated in the mesosphere during the 2019 SH winter, resulting in infrared radiative cooling. Furthermore, CO_2 produces CO through photolysis; however, only a minor amount of CO_2 is involved in the reaction. CO is also injected into the mesosphere from the thermosphere. This suggests that, in the present SSW, the mesospheric cooling occurred because of the combined effects of upward-propagating PWs

and chemical species transport through wave-induced residual mean circulation. Therefore, the present study signifies the effect of anthropogenically emitted greenhouse gases on the upper atmosphere dynamics by inducing more mesospheric cooling during SSWs.
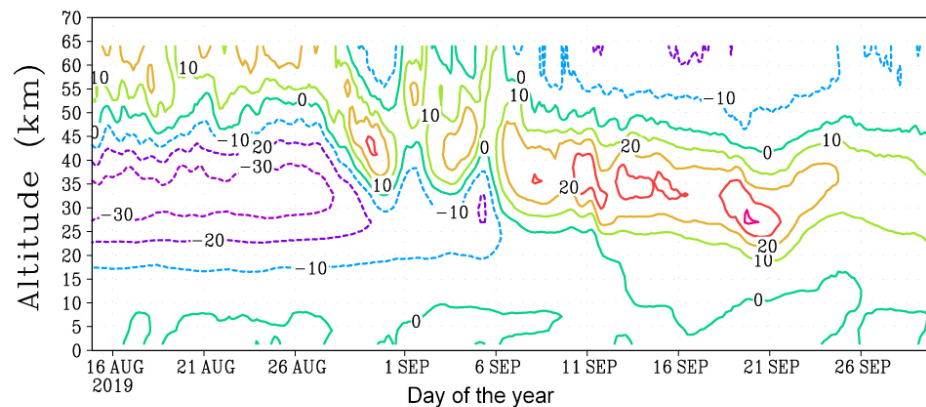

Figure 6. (**a**) Time series of PW1 amplitude between $60°$ and $80°$ S. (**b**) the same but for the PW2 amplitude. (**c**) deviation from the average (August–September) zonal-mean temperature (K).
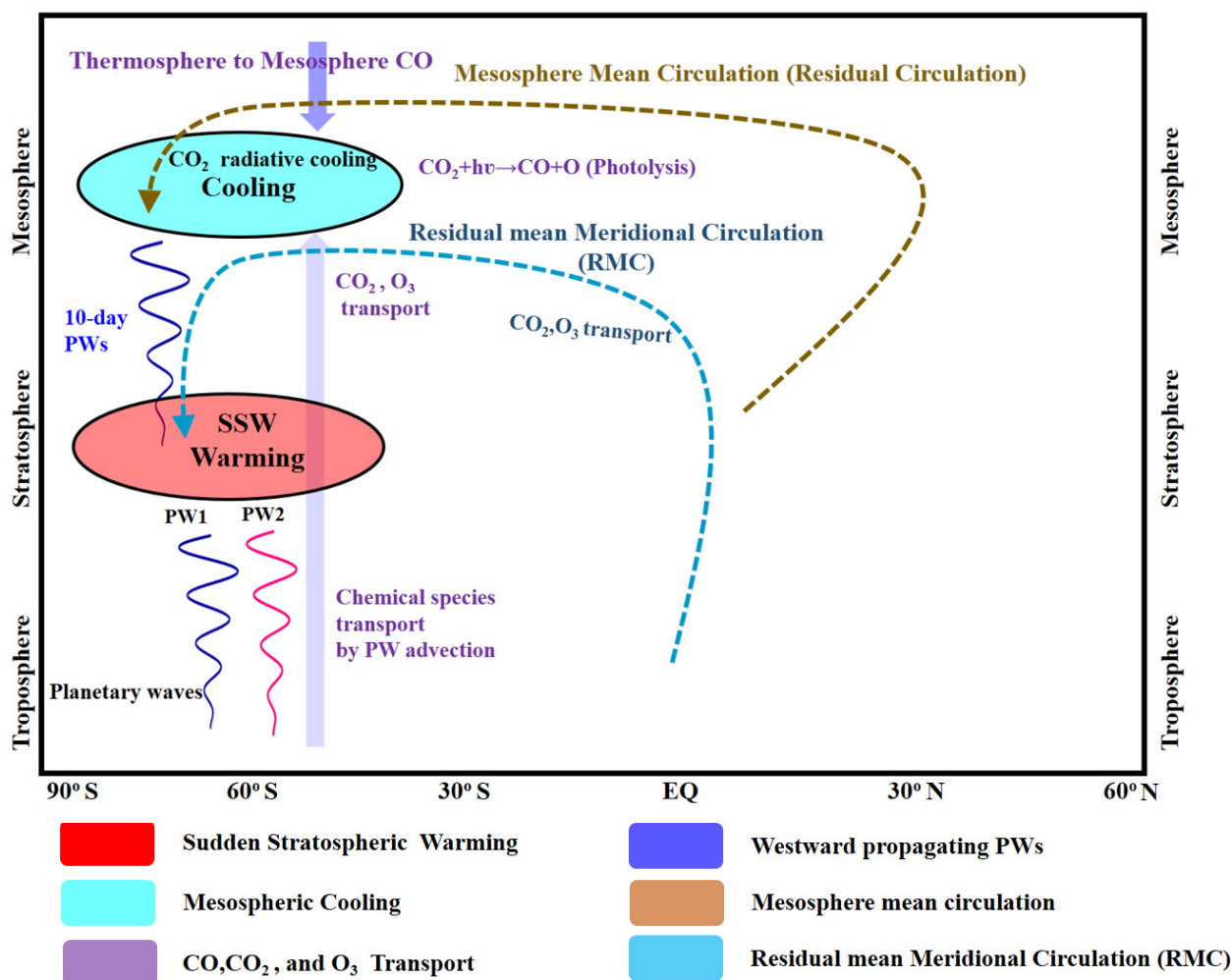
Figure 7. Schematic illustration (not to scale) of SSW effects on the polar mesospheric cooling by planetary wave propagation and chemical species during the 2019 SH minor SSW. (PW = planetary waves, SSW = stratospheric sudden warming).

4. Conclusions

The present communication analyzed the rare occurrence of Antarctic mesospheric cooling during the 2019 minor SSW in the SH using simultaneous observations from the KSS meteor radar in Antarctica (62.22° S, 58.78° W), the MLS satellite, and MERRA data. Effort was made to determine the potential reasons for the unusual mesospheric cooling by examining planetary wave propagation from ground-based radar observations, and the upward and meridional transport of chemical species. We observed 26 K cooling in the Antarctic mesopause and 24 K in the middle mesosphere during the SSW. The 10-day wave oscillations were observed in the temperature from the stratosphere to the mesosphere and in the mesospheric winds. During the SSW, a large enhancement in CO, and anti-correlation with mesospheric temperature were observed. CO enhancement suggests the existence of abundant CO_2 and its infrared cooling effect in the mesosphere. Hence, the highest level of mesospheric cooling could be due to infrared cooling by CO_2, rather than the adiabatic cooling effect of the gravity waves. The estimated residual mean meridional circulation during the SH winter shows the upward and poleward transport of planetary wave-induced eddy circulation cells in the upper stratosphere and lower mesosphere and downward transport in the polar region before the SSW. During the SSW, the eddy vertical velocity is downward in the lower stratosphere causing heating, and upward in the lower mesosphere resulting in cooling. The planetary wave structure and chemical species in the mesosphere indicate that mesosphere cooling can be due to the combined effect of PWs,

and the transport of chemical species through the planetary wave-induced residual mean meridional circulation that exists in the SH. Although this SSW is considered a minor SSW, its effects on the polar mesospheric thermal structure and dynamics resemble those of a major SSW. To the best of our knowledge, this is the first report regarding the observational evidence of Antarctic mesospheric cooling associated with the 2019 SSW involving the troposphere chemistry and the effect of anthropogenically emitted greenhouse gases on upper atmosphere dynamics. Therefore, the present study provides a piece of observational evidence for the recent long-term simulation study about the atmosphere shrinking through mesospheric cooling induced by anthropogenically emitted greenhouse gases [1]. Further widespread observational or simulated analysis studies are suggested to address the effects of the 2019 SH SSW on atmospheric coupling processes and the quantification of mean circulation and chemical transport.

Supplementary Materials: The following supporting information can be downloaded at: https://www.mdpi.com/article/10.3390/atmos13091475/s1, Figure S1: Day-altitude contour of the daily (a) zonal mean temperature deviation (anomalies), (b) zonal mean zonal wind, (c) planetary wave1, and (d) wave2 amplitudes observed in the geopotential heights. All the observations are from August to October 2019. The MERRA data has been used to generate this figure.

Author Contributions: Conceptualization, data curation, writing—original draft preparation; S.E., K.N.K., K.-H.S., M.V.R. (Madineni Venkat Ratnam) and Y.H.K.; methodology, S.E., K.G.; software, validation, formal analysis, S.E., Y.-S.L., J.-Y.H., W.L., M.P., C.K.M., J.-Y.J., A.V.K., G.V.C. and M.V.R. (Mannem Venkatarami Reddy); investigation, S.E., K.N.K., K.-H.S., A.V.K., Y.-S.L. and K.G., resources, K.-H.S.; funding acquisition, K.-H.S. and M.V.R. (Madineni Venkat Ratnam). All authors have read and agreed to the published version of the manuscript.

Institutional Review Board Statement: Not applicable.

Informed Consent Statement: Not applicable.

Data Availability Statement: The meteor radar data used in this study can be obtained from https://doi.org/10.5281/zenodo.6098859. The authors also thank the MLS and MERRA-2 teams for providing the temperature data used in this study. The MLS temperature and chemical species data were obtained from http://dx.doi.org/10.5067/Aura/MLS/DATA2021. The MERRA-2 dataset can be obtained from https://disc.gsfc.nasa.gov/datasets/M2I6NVANA_5.12.4/summary.

Conflicts of Interest: The authors declare no conflict of interest.

References

1. Bailey, S.M.; Thurairajah, B.; Hervig, M.E.; Siskind, D.E.; Russell, J.M.; Gordley, L.L. Trends in the Polar Summer Mesosphere Temperature and Pressure Altitude from Satellite Observations. *J. Atmos. Sol.-Terr. Phys.* **2021**, *220*, 105650. [CrossRef]
2. Scherhag, R. Die explosionsartige Stratospharenerwarmung des Spatwinters 1951–1952. *Ber. Dtsch. Wetterd.* **1952**, *6*, 51–53.
3. Pedatella, N.; Chau, J.; Schmidt, H.; Goncharenko, L.; Stolle, C.; Hocke, K.; Harvey, V.; Funke, B.; Siddiqui, T. *How Sudden Stratospheric Warming Affects the Whole Atmosphere*; Eos: Washington, DC, USA, 2018. [CrossRef]
4. Baldwin, M.P.; Ayarzagüena, B.; Birner, T.; Butchart, N.; Butler, A.H.; Charlton-Perez, A.J.; Domeisen, D.I.V.; Garfinkel, C.I.; Garny, H.; Gerber, E.P.; et al. Sudden Stratospheric Warmings. *Rev. Geophys.* **2021**, *59*, e2020RG000708. [CrossRef]
5. van Loon, H.; Jenne, R.L.; Labitzke, K. Zonal Harmonic Standing Waves. *J. Geophys. Res.* **1973**, *78*, 4463–4471. [CrossRef]
6. Krüger, K.; Naujokat, B.; Labitzke, K. The Unusual Midwinter Warming in the Southern Hemisphere Stratosphere 2002: A Comparison to Northern Hemisphere Phenomena. *J. Atmos. Sci.* **2005**, *62*, 603–613. [CrossRef]
7. Liu, H.L.; Roble, R.G. Dynamical Coupling of the Stratosphere and Mesosphere in the 2002 Southern Hemisphere Major Stratospheric Sudden Warming. *Geophys. Res. Lett.* **2005**, *32*, 1–4. [CrossRef]
8. Eswaraiah, S.; Kim, Y.H.; Hong, J.; Kim, J.H.; Ratnam, M.V.; Chandran, A.; Rao, S.V.B.; Riggin, D. Mesospheric Signatures Observed during 2010 Minor Stratospheric Warming at King Sejong Station (62°S, 59°W). *J. Atmos. Sol.-Terr. Phys.* **2016**, *140*, 55–64. [CrossRef]

9. Eswaraiah, S.; Kim, J.H.; Lee, W.; Hwang, J.; Kumar, K.N.; Kim, Y.H. Unusual Changes in the Antarctic Middle Atmosphere During the 2019 Warming in the Southern Hemisphere. *Geophys. Res. Lett.* **2020**, *47*, e2020GL089199. [CrossRef]

10. Lim, E.P.; Hendon, H.H.; Butler, A.H.; Thompson, D.W.J.; Lawrence, Z.D.; Scaife, A.A.; Shepherd, T.G.; Polichtchouk, I.; Nakamura, H.; Kobayashi, C.; et al. The 2019 Southern Hemisphere Stratospheric Polar Vortex Weakening and Its Impacts. *Bull. Am. Meteorol. Soc.* **2021**, *102*, E1150–E1171. [CrossRef]

11. Lee, W.; Song, I.S.; Kim, J.H.; Kim, Y.H.; Jeong, S.H.; Eswaraiah, S.; Murphy, D.J. The Observation and SD-WACCM Simulation of Planetary Wave Activity in the Middle Atmosphere During the 2019 Southern Hemispheric Sudden Stratospheric Warming. *J. Geophys. Res. Space Phys.* **2021**, *126*, e2020JA029094. [CrossRef]

12. Eswaraiah, S.; Lee, C.; Lee, W.; Kim, Y.H.; Kumar, K.N.; Medineni, V.R. Temperature Tele-Connections between the Tropical and Polar Middle Atmosphere in the Southern Hemisphere during the 2010 Minor Sudden Stratospheric Warming. *Atmos. Sci. Lett.* **2020**, *22*, e1010. [CrossRef]

13. Liu, H.L.; Roble, R.G. A Study of a Self-Generated Stratospheric Sudden Warming and Its Mesospheric-Lower Thermospheric Impacts Using the Coupled TIME-GCM/CCM3. *J. Geophys. Res. Atmos.* **2002**, *107*, ACL 15-1–ACL 15-18. [CrossRef]

14. de Wit, R.J.; Hibbins, R.E.; Espy, P.J.; Orsolini, Y.J.; Limpasuvan, V.; Kinnison, D.E. Observations of Gravity Wave Forcing of the Mesopause Region during the January 2013 Major Sudden Stratospheric Warming. *Geophys. Res. Lett.* **2014**, *41*, 4745–4752. [CrossRef]

15. Coy, L.; Siskind, D.E.; Eckermann, S.D.; McCormack, J.P.; Allen, D.R.; Hogan, T.F. Modeling the August 2002 Minor Warming Event. *Geophys. Res. Lett.* **2005**, *32*, 1–4. [CrossRef]

16. Kogure, M.; Yue, J.; Liu, H. Gravity Wave Weakening During the 2019 Antarctic Stratospheric Sudden Warming. *Geophys. Res. Lett.* **2021**, *48*, e2021GL092537. [CrossRef]

17. Smith, A.K.; López-Puertas, M.; García-Comas, M.; Tukiainen, S. SABER Observations of Mesospheric Ozone during NH Late Winter 2002-2009. *Geophys. Res. Lett.* **2009**, *36*. [CrossRef]

18. Smith, A.K.; Garcia, R.R.; Marsh, D.R.; Richter, J.H. WACCM Simulations of the Mean Circulation and Trace Species Transport in the Winter Mesosphere. *J. Geophys. Res. Atmos.* **2011**, *116*, 1–17. [CrossRef]

19. Smith, A.K. Interactions Between the Lower, Middle and Upper Atmosphere. *Space Sci. Rev.* **2012**, *168*, 1–21. [CrossRef]

20. Butchart, N. The Brewer-Dobson Circulation. *Rev. Geophys.* **2014**, *52*, 157–184. [CrossRef]

21. Koval, A.V.; Chen, W.; Didenko, K.A.; Ermakova, T.S.; Gavrilov, N.M.; Pogoreltsev, A.I.; Toptunova, O.N.; Wei, K.; Yarusova, A.N.; Zarubin, A.S. Modelling the Residual Mean Meridional Circulation at Different Stages of Sudden Stratospheric Warming Events. *Ann. Geophys.* **2021**, *39*, 357–368. [CrossRef]

22. Hernandez, G. Climatology of the Upper Mesosphere Temperature above South Pole (90° S): Mesospheric Cooling during 2002. *Geophys. Res. Lett.* **2003**, *30*, 1–4. [CrossRef]

23. Azeem, S.M.I.; Talaat, E.R.; Sivjee, G.G.; Yee, J.H. Mesosphere and Lower Thermosphere Temperature Anomalies during the 2002 Antarctic Stratospheric Warming Event. *Ann. Geophys.* **2010**, *28*, 267–276. [CrossRef]

24. Lee, C.; Kim, J.H.; Jee, G.; Lee, W.; Song, I.S.; Kim, Y.H. New Method of Estimating Temperatures near the Mesopause Region Using Meteor Radar Observations. *Geophys. Res. Lett.* **2016**, *43*, 10580–10585. [CrossRef]

25. Livesey, N.J.; Read, W.G.; Wagner, P.A.; Lambert, A.; Froidevaux, L.; Manney, G.L.; Pumphrey, H.C.; Millan Valle, L.F.; Santee, M.L.; Schwartz, M.J.; et al. *Earth Observing System (EOS), Aura Microwave Limb Sounder (MLS), Version 4.2x Level 2 and 3 Data Quality and Description Document*; Techical Report JPL D-33509; Jet Propulsion Laboratory: Pasadena, CA, USA, 2020.

26. Gelaro, R.; McCarty, W.; Suárez, M.J.; Todling, R.; Molod, A.; Takacs, L.; Randles, C.A.; Darmenov, A.; Bosilovich, M.G.; Reichle, R.; et al. The Modern-Era Retrospective Analysis for Research and Applications, Version 2 (MERRA-2). *J. Clim.* **2017**, *30*, 5419–5454. [CrossRef]

27. Siskind, D.E.; Coy, L.; Espy, P. Observations of Stratospheric Warmings and Mesospheric Coolings by the TIMED SABER Instrument. *Geophys. Res. Lett.* **2005**, *32*, 1–4. [CrossRef]

28. Laštovička, J. A Review of Recent Progress in Trends in the Upper Atmosphere. *J. Atmos. Solar-Terrestrial Phys.* **2017**, *163*, 2–13. [CrossRef]

29. Khosravi, R.; Brasseur, G.; Smith, A.; Rusch, D.; Walters, S.; Chabrillat, S.; Kockarts, G. Response of the Mesosphere to Human-Induced Perturbations and Solar Variability Calculated by a 2-D Model. *J. Geophys. Res. Atmos.* **2002**, *107*, ACH 7-1–ACH 7-21. [CrossRef]

30. Garcia, R.R.; López-Puertas, M.; Funke, B.; Marsh, D.R.; Kinnison, D.E.; Smith, A.K.; González-Galindo, F. On the Distribution of CO_2 and CO in the Mesosphere and Lower Thermosphere. *J. Geophys. Res.* **2014**, *119*, 5700–5718. [CrossRef]

31. Qian, L.; Marsh, D.; Merkel, A.; Solomon, S.C.; Roble, R.G. Effect of Trends of Middle Atmosphere Gases on the Mesosphere and Thermosphere. *J. Geophys. Res. Space Phys.* **2013**, *118*, 3846–3855. [CrossRef]

32. Espy, P.J.; Hibbins, R.E.; Jones, G.O.L.; Riggin, D.M.; Fritts, D.C. Rapid, Large-Scale Temperature Changes in the Polar Mesosphere and Their Relationship to Meridional Flows. *Geophys. Res. Lett.* **2003**, *30*, 1–4. [CrossRef]

33. Torrence, C.; Compo, G.P. A Practical Guide to Wavelet Analysis. *Bull. Am. Meteorol. Soc.* **1998**, *79*, 61–78. [CrossRef]

34. Shen, X.; Wang, L.; Osprey, S. Tropospheric Forcing of the 2019 Antarctic Sudden Stratospheric Warming. *Geophys. Res. Lett.* **2020**, *47*, e2020GL089343. [CrossRef]

35. Wang, J.C.; Palo, S.E.; Forbes, J.M.; Marino, J.; Moffat-Griffin, T.; Mitchell, N.J. Unusual Quasi 10-Day Planetary Wave Activity and the Ionospheric Response During the 2019 Southern Hemisphere Sudden Stratospheric Warming. *J. Geophys. Res. Space Phys.* **2021**, *126*, e2021JA029286. [CrossRef]

36. Emmert, J.T.; Stevens, M.H.; Bernath, P.F.; Drob, D.P.; Boone, C.D. Observations of Increasing Carbon Dioxide Concentration in Earth's Thermosphere. *Nat. Geosci.* **2012**, *5*, 868–871. [CrossRef]

37. Andrews, D.; Leovy, C.; Holton, J. *Middle Atmosphere Dynamics*; Academic Press: Orlando, FL, USA, 1987.

38. Holton, J.R. *An Introduction to Dynamic Meteorology*, 4th ed.; Elsevier Academic Press: Washington, DC, USA, 2004; p. 553.

39. Clark, J.H.E.; Rogers, T.G. The transport of conservative trace gases by planetary waves. *J. Atmos. Sci.* **1978**, *35*, 2232–2235. [CrossRef]

40. Lim, E.-P.; Hendon, H.H.; Boschat, G.; Hudson, D.; Thompson, D.W.J.; Dowdy, A.J.; Arblaster, J.M. Australian Hot and Dry Extremes Induced by Weakenings of the Stratospheric Polar Vortex. *Nat. Geosci.* **2019**, *12*, 896–901. [CrossRef]

41. Menviel, L.; Spence, P.; Yu, J.; Chamberlain, M.A.; Matear, R.J.; Meissner, K.J.; England, M.H. Southern Hemisphere Westerlies as a Driver of the Early Deglacial Atmospheric CO_2 Rise. *Nat. Commun.* **2018**, *9*, 2503. [CrossRef]

42. Kouker, W.; Brasseur, G. Transport of Atmospheric Tracers by Planetary Waves During A Winter Stratospheric Event: A Three-Dimensional Model Simulation. *J. Geophys. Res.* **1986**, *91*, 13167–13185. [CrossRef]